



Room temperature annealing of SnS₂ films with electron impulse force

Nahid Sultan Al-Mamun^a, Douglas E. Wolfe^b, Aman Haque^{a,*}, Jae-Gyun Yim^{c,d},
Seong Keun Kim^{c,d}

^a Department of Mechanical Engineering, Penn State University, University Park, PA 16802, USA

^b Department of Materials Science & Engineering, Penn State University, University Park, PA 16802, USA

^c Electronic Materials Research Center, Korea Institute of Science and Technology, Seoul 02791, South Korea

^d KU-KIST Graduate School of Converging Science and Technology, Korea University, Seoul 02841, South Korea

ARTICLE INFO

Keywords:

Atomic layer deposition

Annealing

Electromigration

Transmission electron microscopy

ABSTRACT

Tin disulfide (SnS₂) is a layered metal dichalcogenide material with wide bandgap favoring electronics, sensors, photovoltaics, and water splitting applications. Atomic layer deposition can precisely control film thickness over large area, which is important for device applications. The as-deposited SnS₂ shows poor crystallinity, which is difficult to anneal with high temperature because of de-sulfurization. We demonstrate room temperature annealing by exploiting electron impulse force. High current density pulses were applied with very low duty cycle to suppress heat accumulation, while the momentum of the electron pulses interacted with the defects and grain boundaries. For seven-layer thick tin di-sulfide specimens, resistivity was decreased by ten times at ambient temperature. Enhancement of crystallinity was analyzed with Raman spectroscopy and transmission electron microscopy followed by geometric phase analysis. The demonstrated technique can impact applications where post-synthesis annealing requires high temperature and special environment.

Tin disulfide (SnS₂) is a layered metal dichalcogenide materials with crystal structure similar to transition metal dichalcogenides, but with significantly wider (~2.2 eV, indirect) bandgap [1]. The wider bandgap is expected to favor applications in field effect transistors [2]. It is also used in lithium-sulfur or sodium ion battery electrodes [3,4]. Two-dimensional version of SnS₂ enable unique device features, such as non-planarity [5] and atomically seamless in-plane heterostructure [6]. The optical absorptivity of SnS₂ area attractive for hydrogen production (anode material for photoelectrochemical water splitting [7]) and for photovoltaic devices [8]. In all these applications, oxidation resistance of SnS₂ is noted to be a unique aspect that leads to device performance stability and robustness [9]. Another long term benefit is the sustainability of the material with remarkable advantages of low cost and naturally occurring abundance with no adverse environmental concerns [10].

The motivation of this study comes from the importance of control of crystallinity, layer/thickness and large area coverage of two-dimensional materials [11], preferably at low processing temperatures [12]. Mechanical exfoliation has played dominant role in almost all 2D materials studied so far and SnS₂ is not an exception [13]. This has been extended to liquid/chemical [9,14] exfoliation for increase in yield

and/or reduced cost and efforts. While exfoliation produces better crystal quality, the coverage area and uniformity of layers are difficult to control. Chemical vapor deposition (CVD) significantly improves these drawbacks [2], at the cost of high (450–650 °C) processing temperatures. Atomic layer deposition (ALD) also uses gas precursors, but at lower (150–250 °C) temperatures. The unique advantages of ALD are superior layer uniformity and conformal coverage over large area [5, 15]. However, the process yields lower crystallinity compared to the CVD [16]. Therefore, ALD-based synthesis is typically followed by thermal annealing. It is important to note that higher annealing temperatures may not necessarily be conducive for SnS₂ because of materials loss by thermal re-evaporation [17]. Similar results are reported for thermally evaporated SnS₂, showing 300 °C annealing producing better results than 500 °C [18]. In general, low temperature synthesis implies higher surface quality while low temperature annealing obviates the need for special annealing conditions (e.g., sulfur powder or H₂S [19] for SnS₂).

In this study, we propose a novel annealing procedure, where the average temperature is maintained near ambient. Here, very low duty cycle electrical pulses with high current density are passed through the material. The current pulses produce two effects, (a) Joule heat and (b)

* Corresponding author.

E-mail address: mah37@psu.edu (A. Haque).

<https://doi.org/10.1016/j.scriptamat.2022.115107>

Received 5 September 2022; Received in revised form 8 October 2022; Accepted 10 October 2022

Available online 19 October 2022

1359-6462/© 2022 Acta Materialia Inc. Published by Elsevier Ltd. All rights reserved.

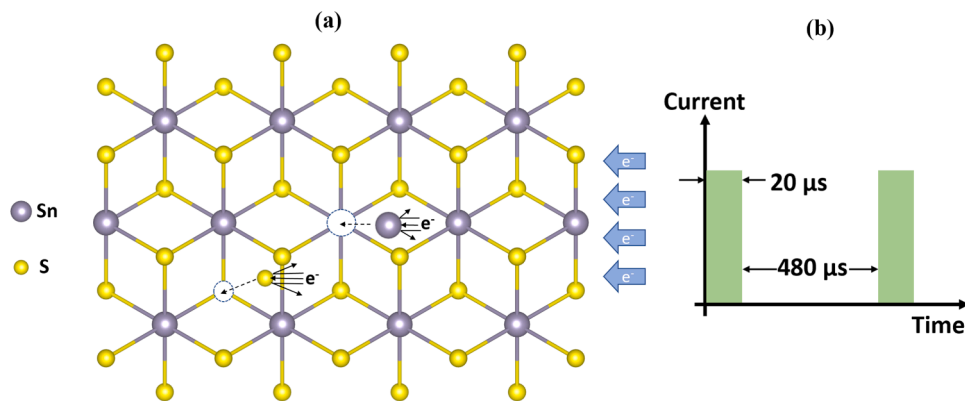


Fig. 1. (a) Schematic illustration of electron wind force induced defect mobilization resulting from interaction between a defect and a high energy electron (b) Low duty cycle current pulsing scheme for electron impulse force annealing.

the electron wind force. Joule heating arises primarily due to the scattering of the electrons by the ordered lattice atoms. The electron wind force, on the other hand, is non-thermal and mechanical in nature. It is developed when the momentum of the electron is transferred to the defective atoms upon impact in the solid. For electron conducting materials, the electron wind force is estimated from the semi-classical model due to Huntington and Grone [20] or the quantum mechanical

model due to Bosvieux and Friedel [21,22]. The specimen material (SnS₂) has appreciable density of free electrons. This is validated from our electrical conductivity measurement at a later section as well as electrode applications in the literature [7,8]. Fig. 1a schematically shows the scattering of the high energy electrons supplied from the current pulses as they encounter defective regions. This is an approximate depiction of defects in SnS₂, however, more accurate defect

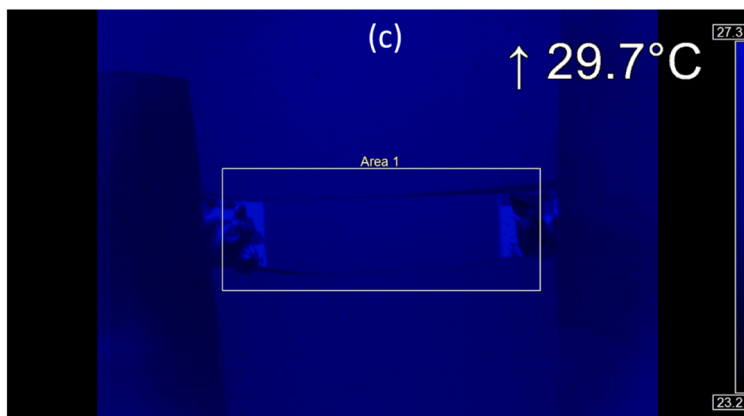
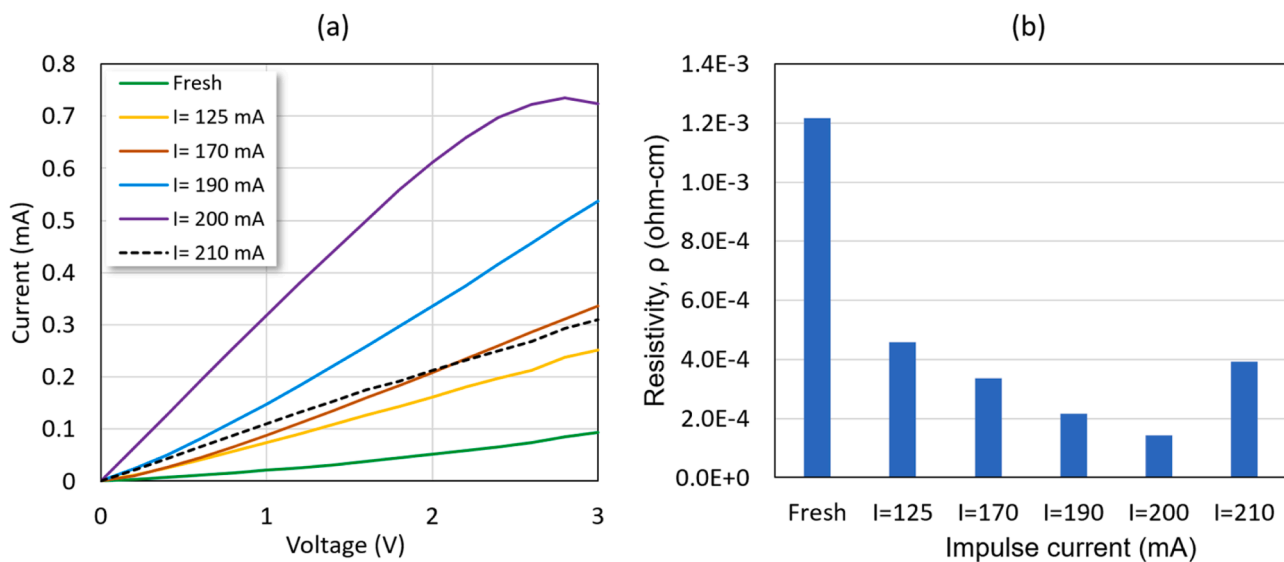


Fig. 2. (a) Effect of pulsed current density on the current-voltage sweep curves and (b) corresponding resistivity of ALD SnS₂ specimens (c) Thermal microscope image showing room temperature annealing.

configuration can be obtained with molecular dynamics models. The fundamental mechanics is sufficiently described by Huntington-Grone model. There is also strong similarity with classical electromigration, where the Joule heating increasingly worsens the microstructure by generating new defects and voids via thermo-mechanical stresses. The synergy of current density, mechanical stress, and temperature spirals out towards a thermal runaway in electromigration. The basic difference in our proposed process is that we control the temperature by very low frequency current pulses with very small pulse width. This is shown in Fig. 1b. If the duty cycle is very low, the pulses keep on applying impulsive forces on the defects to mobilize them, where the temperature rise is suppressed. In absence of significant temperature rise, it is possible to increase the current density to a level where the defects have enough mobility to escape the material.

To investigate the effectiveness of electron impulse force induced annealing at room temperature, we synthesized few-layer SnS₂ with ALD process. Large area (2 × 2 cm²) specimens were prepared on Al₂O₃/SiO₂/Si substrates. The SnS₂ layers were grown by a two-step process. First, 1 monolayer SnS₂ was grown at 150 °C, and followed by the ALD growth of the main layer at 240 °C. The as-grown SnS₂ has approximately seven monolayers. An ALD cycle consists of Sn precursor feeding (2 s) – purge (10 s) – H₂S plasma (2 s) – purge (20 s) steps. Bis(1-dimethylamino-2-methyl-2-propoxy) tin(II) and H₂S plasma with a RF power of 150 W were used as the Sn and S precursors, respectively. The specimen was then mounted on a current pulse generator comprised of a Sorensen DCS 100–12E DC power supply, a Northrop Grumman eDrive™ Laser System Controller as pulse generator and a Rigol DS 1104 oscilloscope. The specimen temperature was monitored with an Optris PI-640 thermal microscope. To minimize temperature rise, the lowest pulse width and frequency (20 μs and 2 Hz respectively) were used as the optimum current value was experimentally determined to be 0.2 A. For a 4 nm thick specimen, this results in 2.5 × 10⁶ A/cm² current density. For these processing parameters, the specimen temperature essentially remained at the ambient. Such temperature suppression helps prevention of any thermal runaway during the high current density electro-pulsing experiments. A four-point probing setup was used to measure the specimen resistance.

Crystallinity can be experimentally measured via Raman spectroscopy, grazing incidence X-ray diffraction, high resolution transmission or scanning microscopy techniques. Another technique is measurement of electrical properties, which strongly depend on crystallinity. Defects and interfaces, such as grain boundaries or layer discontinuities scatter electron to reduce the mobility (or increase the resistivity). This is particularly true for nanocrystalline materials, for which decrease of grain size from 100 nm to 10 nm increases the volume fraction of grain boundaries from 7% to 25% [23]. Remarkably similar scaling effect in resistivity of nanocrystalline metals is reported in the literature showing highly non-linear increase in the resistivity as grain size becomes comparable to the electron mean free path [24]. The relevant grain size range for ALD-synthesized SnS₂ is about 5–20 nm [2,5,16,19,25]. We therefore expect very strong grain size effect on electrical resistivity.

Fig. 2a shows the I-V curves for the ~4 nm thick (~seven-layers) SnS₂ specimens. Here, the first curve is for the as-deposited specimen before any annealing. The response to the electron impulse force annealing is shown by the various amplitudes of current pulses, each for 20 s duration and 2 Hz frequency. Fig. 2b shows the resistivity as function of annealing current pulse amplitudes. Appreciable improvement in electrical conductivity is observed as the pulse current amplitude is increased. For pulsed current of 200 mA (current density = 2.5 × 10⁶ A/cm²), we observed the highest decrease in resistivity (more than ten times decrease compared to the as received SnS₂), which indicates increase in crystalline quality. At this current density, the forward current-voltage curve shows saturation, indicating the limit to the effectiveness of the annealing technique. This is the point where the electron impulse force annealing process also starts creating new defects. It is confirmed by the output from the pulsed current of 210 mA,

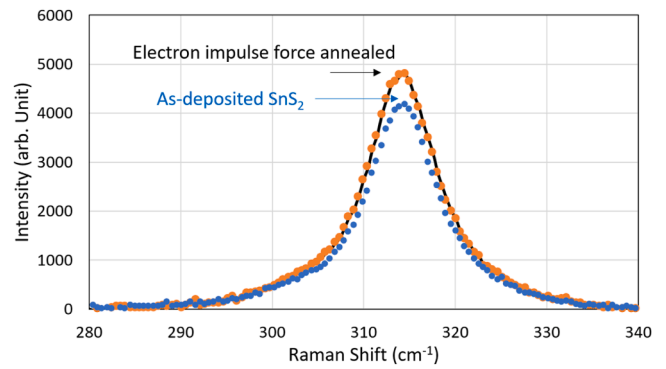


Fig. 3. Raman spectra of as-deposited SnS₂ and room temperature annealed SnS₂ using electron impulse current.

where the trend in resistivity reverses, i.e., increases from 1.42 × 10⁻⁴ to 3.91 × 10⁻⁴ ohm-cm. This is probably due to the increase in temperature that creates more new defects in the material compared to the electron impulse annealing process. It is possible to anneal the specimens further, however the setup will require low temperature specimen stage or even lower duty cycle pulsed current source. Fig. 2c shows the effective temperature of the specimen during annealing with the 200 mA current pulses. Essentially, the specimen temperature remains at the ambient. This is the unique feature of electrical impulse force annealing, compared to conventional process that requires up to 350 °C.

Raman spectroscopy is another well-established characterization technique for 2D materials. We acquired high-resolution Raman spectra using Horiba LabRAM HR Evolution with 100X, NA = 0.9 microscope objective equipped with 532 nm green laser and 1800 gm/mm grating. For the as-received ALD specimens, the Raman spectra show a peak at 314 cm⁻¹. This is the characteristic signal for the A_{1g} mode, which is related to out of plane vibration of sulfur atoms. The data was collected from several random locations and the similarities of the peak intensities suggest uniformity of the SnS₂ specimens. Fig. 3 shows the Raman spectra before and after electron impulse force annealing. Literature indicates increase in intensity (or decrease in the full width at half maximum) following high temperature annealing [2,5,17]. Our experimental result is therefore consistent with the literature, even though this study is performed at room temperature only. It is important to note that no peak shift (increase or decrease in stress) but only peak narrowing is expected. We did not observe any in-plane vibrational mode (E_{2g}) at 208 cm⁻¹, which is also consistent with the literature.

To explain why the mechanical force obtained from the high-density electrical pulse is able to mobilize the defects, we estimate the supplied external energy and compare that with the activation energy for defect mobilization. In order to roughly quantify the electron wind force or stress generated on each atom for the range of current density used in this study, we used following equation [26,27] based on Huntington-Grone model [20]:

$$F = z^* \times e \times \rho \times j$$

where, z^* is the effective valence charge, e is the electron charge, ρ is the resistivity, and j is the current density. Assuming Sn is the primary source of the free electrons in SnS₂ system, we considered z^* as -35.34 [27]. For a current density of 1.56 × 10⁶ to 2.5 × 10⁶ A/cm², the estimated wind force varies from 0.2 to 0.4 fN (femto Newton), which corresponds to ~3 to 6.5 kPa and ~6 to 11 kPa of stress acting on per Sn and S atoms, respectively. For defect mobilization activation, we estimated the stress required to move a single dislocation of SnS₂ using the Peierls-Nabarro model [28] using following equation [29]:

$$\tau = \frac{2G}{1 - \nu} \exp\left(\frac{-2\pi d}{(1-\nu)b}\right)$$

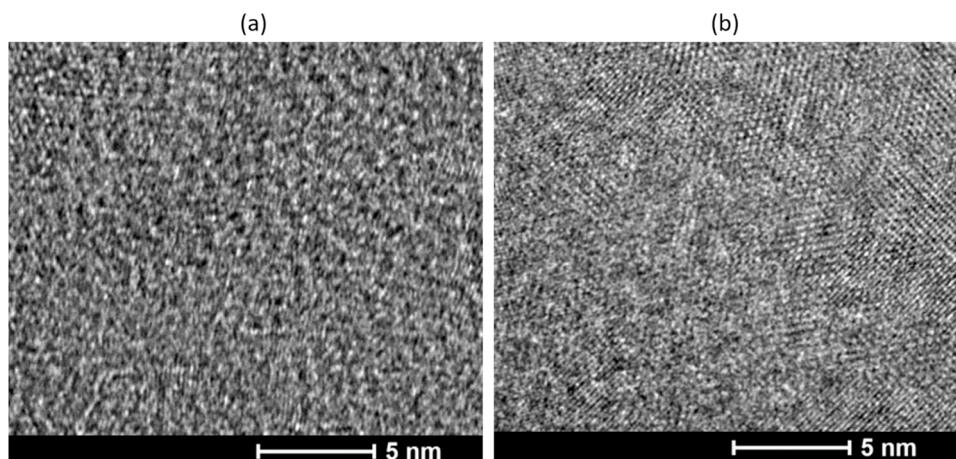


Fig. 4. TEM images of 5 nm thick ALD SnS₂ in (a) as-deposited and (b) electron wind force annealed conditions.

where, G is shear modulus (25.3 GPa [30]), ν is the Poisson's ratio (0.24 [30]), d is the interplanar spacing (0.32 nm [1,31]), and b is the slip distance (0.15 nm, considering [001] basal plane slip associated with [110] type dislocations). The estimated shear stress value was calculated to be ~ 1.5 kPa, which is smaller than the electron wind stress acting on per atom. Therefore, it can be assumed that the generated electron wind force is strong enough to induce mobility of defects in SnS₂. However, this estimated wind force value can vary depending on the scattering angle or cross section, crystal lattice direction, and position of the atoms in the lattice with respect to its equilibrium position [26,32]. These factors contribute to the net scattering potential acting on the defects controlling the direction of motion of the defects. It is important to note that according to Huntington-Groene model, the momentum transfer due to scattering of electrons occurs only in defect sites and have negligible impact on the crystal lattice. The response of the defects will vary depending on the atom's locations in different sites, i.e., point defects, dislocations, and grain boundaries. The scattering of electrons is expected to be more intense at the grain boundaries due to higher density of defects at the grain boundaries, which may facilitate electron interaction with more than a single scatterer resulting in more efficient momentum transfer [33].

To obtain visual information on the crystallinity enhancement due to the electrical impulse force, we performed transmission electron microscopy (TEM) on both as-received and annealed specimens. Most of the studies on SnS₂ synthesis show cross-sectional TEM images that discern the individual layers. However, cross-sectional specimens do not accurately capture information on grain size or the local defects in the grains, as obtained from the plan-view. Therefore, we prepared the TEM

specimens by first spin coating a thin layer of polymethyl methacrylate (PMMA) on SnS₂ samples and then used hydrofluoric acid (16.7%) to etch the substrate. This floats off the specimens which were captured on TEM grids followed by rinsing with deionized water and drying at 70 °C. Subsequently, the PMMA layer was removed using gentle acetone and Isopropyl alcohol washing. The TEM bright field images were acquired using FEI Talos F200X TEM system at 200 kV.

Fig. 4 shows the TEM images of the SnS₂ specimen before and after the electron wind force annealing at room temperature. The as-deposited specimen looks mostly amorphous with small areas indicative of crystalline order in atoms. This could be due to the characteristic feature of a two-step ALD process, where an amorphous underlayer is seen below nanocrystalline flakes [5]. The electron impulse force annealing appears to enhance the crystallinity significantly, but it remains difficult to estimate long range of crystallinity of the grain size. The factor that obfuscates this is the possible presence of PMMA contaminants on the specimens. To better estimate the grain size, we performed geometric phase analysis (GPA) [34]. This technique is more commonly used to perform strain analysis in crystalline materials and is particularly useful in identifying regions of localized defects and the grain boundaries. The atomic strain mapping (ϵ_{xx}) of as-deposited and electron wind force annealed SnS₂ samples are shown in Fig. 5. Fig. 5 elucidates the crystallinity better than the Fig. 4 by highlighting the local strain (defects and interfaces) regions. The GPA technique shows dislocations by red-blue combination to represent the co-existing tension and compression because of the extra atomic plane. Therefore, they can indicate presence of dislocation and grain boundaries by visualizing their associated strain maps. The dislocation densities of samples were

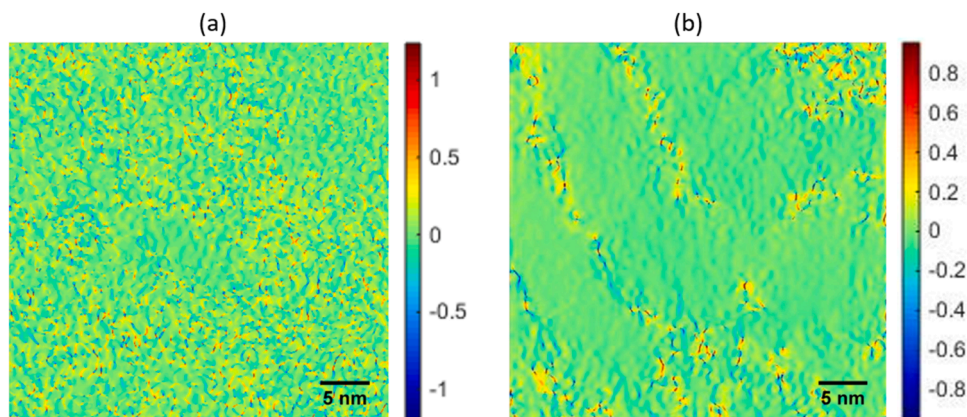


Fig. 5. Strain mapping (ϵ_{xx}) of the (a) as-deposited and (b) electron wind force annealed samples, obtained by Geometric phase analysis of the TEM images.

estimated from the corresponding strain maps using the public domain ImageJ software. The dislocation density of the as-deposited sample was found to be approximately 7.8×10^{17} counts/m², whereas the corresponding value for the electron impulse force annealed sample was estimated to be 1.9×10^{17} counts/m². In addition, relatively larger crystallites are seen in the electron wind force annealed specimens (Fig. 5b), which explains the 10 times decrease in specimen resistivity (Fig. 2).

In this study, we demonstrate a room temperature annealing process on atomic layer deposited few-layers of SnS₂. The crystallinity of the as-deposited materials is apparently low due to the processing conditions. We then enhance the crystallinity with a novel electron impulse annealing process that works at room temperature. Here, the interaction between electron and defect is exploited to impart a mechanical force on the defects to mobilize them. The temperature rise due to Joule heating is suppressed by supplying the current in very low duty cycle pulses. The forward current-voltage sweep data indicates about 10 times improvement in specimen resistivity. This is supported by Raman spectroscopy and TEM visualization techniques. The demonstrated technique can potentially eliminate the need for high temperature and special environment (such as sulfur in case of SnS₂) annealing of 2D materials.

Declaration of Competing Interest

The authors declare that they have no known competing financial interests or personal relationships that could have appeared to influence the work reported in this paper.

Acknowledgments

This work was partially supported by the US National Science Foundation (ECCS # 2015795). We also acknowledge the support from Defense Threat Reduction Agency (DTRA) as part of the Interaction of Ionizing Radiation with Matter University Research Alliance (IIRM-URA) under Contract No. HDTRA1–20–2-0002. The content of the information does not necessarily reflect the position or the policy of the federal government, and no official endorsement should be inferred.

References

- [1] Y. Huang, E. Sutter, J.T. Sadowski, M. Cotlet, O.L.A. Monti, D.A. Racke, M. R. Neupane, D. Wickramaratne, R.K. Lake, B.A. Parkinson, P. Sutter, Tin disulfide—an emerging layered metal dichalcogenide semiconductor: materials properties and device characteristics, *ACS Nano* 8 (10) (2014) 10743–10755.
- [2] L. Xu, P. Zhang, H. Jiang, X. Wang, F. Chen, Z. Hu, Y. Gong, L. Shang, J. Zhang, K. Jiang, J. Chu, Large-scale growth and field-effect transistors electrical engineering of atomic-layer SnS₂, *Small* 15 (46) (2019), 1904116.
- [3] W. Jun, C. Bing, L. Qingqing, H. Ailin, L. Xiaoying, J. Qi, Preparing a composite including SnS₂, carbon nanotubes and S and using as cathode material of lithium-sulfur battery, *Scr. Mater.* 177 (2020) 208–213.
- [4] Z. Li, J. Zheng, M. Xiao, H. Jiang, L. Wang, H. Song, H.-H. Gao, Three-dimensional 1T-SnS₂ wrapped with graphene for sodium-ion battery anodes with highly reversible sodiation/desodiation, *Scr. Mater.* 211 (2022), 114500.
- [5] J.J. Pyeon, I.H. Baek, W.C. Lee, H. Lee, S.O. Won, G.Y. Lee, T.M. Chung, J.H. Han, S.H. Baek, J.S. Kim, J.W. Choi, C.Y. Kang, S.K. Kim, Wafer-scale, conformal, and low-temperature synthesis of layered tin disulfides for emerging nonplanar and flexible electronics, *ACS Appl. Mater. Interfaces* 12 (2) (2020) 2679–2686.
- [6] Y.J. Gong, H.T. Yuan, C.L. Wu, P.Z. Tang, S.Z. Yang, A.K. Yang, G.D. Li, B.F. Liu, J. van de Groep, M.L. Brongersma, M.F. Chisholm, S.C. Zhang, W. Zhou, Y. Cui, Spatially controlled doping of two-dimensional SnS₂ through intercalation for electronics, *Nat. Nanotechnol.* 13 (4) (2018) 294–299.
- [7] L. Chen, E. Liu, F. Teng, T. Zhang, J. Feng, Y. Kou, Q. Sun, J. Fan, X. Hu, H. Miao, Two-dimensional SnS₂ nanosheets arrays as photoelectrode by low temperature CVD method for efficient photoelectrochemical water splitting, *Appl. Surf. Sci.* 467–468 (2019) 698–707.
- [8] R.E. Banai, J.C. Cordell, G. Lindwall, N.J. Tanen, S.L. Shang, J.R. Nasr, Z.K. Liu, J. R.S. Brownson, M.W. Horn, Control of phase in tin sulfide thin films produced via rf-sputtering of SnS₂ target with post-deposition annealing, *J. Electron. Mater.* 45 (1) (2016) 499–508.
- [9] T. Feng, D. Zhang, X. Li, Q. Abdul, Z. Shi, J. Lu, P. Guo, Y. Zhang, J. Liu, Q.J. Wang, SnS₂ nanosheets for er-doped fiber lasers, *ACS Appl. Nano Mater.* 3 (1) (2020) 674–681.
- [10] M. Liu, H. Wu, X. Liu, Y. Wang, M. Lei, W. Liu, W. Guo, Z. Wei, Optical properties and applications of SnS₂SAs with different thickness, *Opto Electron. Adv.* 4 (10) (2021), 200029-1-200029-10.
- [11] Z. Lin, A. McCreary, N. Briggs, S. Subramanian, K. Zhang, Y. Sun, X. Li, N.J. Borys, H. Yuan, S.K. Fullerton-Shirey, A. Chernikov, H. Zhao, S. McDonnell, A. M. Lindenberg, K. Xiao, B.J. LeRoy, M. Drndić, J.C.M. Hwang, J. Park, M. Chhowalla, R.E. Schaak, A. Javey, M.C. Hersam, J. Robinson, M. Terrones, 2D materials advances: from large scale synthesis and controlled heterostructures to improved characterization techniques, defects and applications, *2D Mater.* 3 (4) (2016), 042001.
- [12] H. Xu, J. Xing, J.h. Lu, X. Han, D. Li, Z. Zhou, L.H. Bao, H.J. Gao, Y. Huang, Annealing effects on the electrical and photoelectric performance of SnS₂ field-effect transistor, *Appl. Surf. Sci.* 484 (2019) 39–44.
- [13] J. Liu, C. Xia, H. Li, A. Pan, High on/off ratio photosensitive field effect transistors based on few layer SnS₂, *Nanotechnology* 27 (34) (2016) 34LT01.
- [14] X. Ma, Z. Xie, Z. Yang, G. Zeng, M. Xue, X. Zhang, Inkjet printed 2D SnS₂ nanosheets for ammonia gas sensor, *Mater. Res. Express* 6 (1) (2018), 015025.
- [15] J. Cai, X. Han, X. Wang, X. Meng, Atomic layer deposition of two-dimensional layered materials: processes, *Growth Mech. Charact. Matter* 2 (3) (2020) 587–630.
- [16] M. Mattinen, P.J. King, L. Khriachtchev, K. Meinander, J.T. Gibbon, V.R. Dhanak, J. Räsänen, M. Ritala, M. Leskelä, Low-temperature wafer-scale deposition of continuous 2D SnS₂ films, *Small* 14 (21) (2018), 1800547.
- [17] G. Ham, S. Shin, J. Park, J. Lee, H. Choi, S. Lee, H. Jeon, Engineering the crystallinity of tin disulfide deposited at low temperatures, *RSC Adv.* 6 (59) (2016) 54069–54075.
- [18] K. Anlin Lazar, V.J. Cicily Rigi, D. Divya, K.J. Saji, Effect of annealing on structural and optical properties of SnS₂ thin films grown by thermal evaporation and post sulphur annealing technique, *IOP Conf. Ser. Mater. Sci. Eng.* 1166 (1) (2021), 012004.
- [19] S. Lee, S. Shin, G. Ham, J. Lee, H. Choi, H. Park, H. Jeon, Characteristics of layered tin disulfide deposited by atomic layer deposition with H₂S annealing, *AIP Adv.* 7 (4) (2017), 045307.
- [20] H.B. Huntington, A.R. Grone, Current-induced marker motion in gold wires, *J. Phys. Chem. Solids* 20 (1) (1961) 76–87.
- [21] C. Bosvieux, J. Friedel, Sur l'électrolyse des alliages métalliques, *J. Phys. Chem. Solids* 23 (1) (1962) 123–136.
- [22] A. Lodder, Calculations of the screening of the charge of a proton migrating in a metal, *Phys. Rev. B* 74 (4) (2006), 045111.
- [23] G. Palumbo, S.J. Thorpe, K.T. Aust, On the contribution of triple junctions to the structure and properties of nanocrystalline materials, *Scr. Metall. Mater.* 24 (7) (1990) 1347–1350.
- [24] I. Bakonyi, Accounting for the resistivity contribution of grain boundaries in metals: critical analysis of reported experimental and theoretical data for Ni and Cu, *Eur. Phys. J. Plus* 136 (4) (2021) 410.
- [25] N. Lee, G. Lee, H. Choi, H. Park, Y. Choi, H. Seo, H. Ju, S. Kim, O. Sul, J. Lee, S.-B. Lee, H. Jeon, Layered deposition of SnS₂ grown by atomic layer deposition and its transport properties, *Nanotechnology* 30 (40) (2019), 405707.
- [26] J.P. Dekker, A. Lodder, J. van Ek, Theory for the electromigration wind force in dilute alloys, *Phys. Rev. B* 56 (19) (1997) 12167–12177.
- [27] Y.C. Liu, B. Afflerbach, R. Jacobs, S.K. Lin, D. Morgan, Exploring effective charge in electromigration using machine learning, *MRS Commun.* 9 (2) (2019) 567–575.
- [28] F.R.N. Nabarro, Fifty-year study of the Peierls-Nabarro stress, *Mater. Sci. Eng. A* 234–236 (1997) 67–76.
- [29] T. Suzuki, S. Takeuchi, Correlation of peierls-nabarro stress with crystal structure, *Rev. Phys. Appl.* 23 (4) (1988) 685 (Paris).
- [30] Z.Q. Zhen, H.Y. Wang, Density functional study of the electronic, elastic, and lattice dynamic properties of SnS₂, *Acta. Phys. Pol. A* 137 (6) (2020).
- [31] Y. Sun, H. Cheng, S. Gao, Z. Sun, Q. Liu, Q. Liu, F. Lei, T. Yao, J. He, S. Wei, Y. Xie, Freestanding tin disulfide single-layers realizing efficient visible-light water splitting, *Angew. Chem. Int. Ed.* 51 (35) (2012) 8727–8731.
- [32] R.S. Sorbello, A. Lodder, S.J. Hoving, Finite-cluster description of electromigration, *Phys. Rev. B* 25 (10) (1982) 6178–6187.
- [33] R. Dannenberg, A.H. King, Grain boundary resistivity and electrically induced grain boundary migration (EIGM) in metallic bamboo microstructures, *Interface Sci.* 7 (1) (1999) 33–44.
- [34] S. Feng, Z. Xu, Strain characterization in two-dimensional crystals, *Materials* 14 (16) (2021).